# Effects of saltwater infiltration on nested groundwater flow systems

Xiaolang Zhang[1], Jiu Jimmy Jiao[2], Xin Luo[2], Hailong Li[3], and Xingxing Kuang[3]

[1]The University of Hong Kong
[2]University of Hong Kong
[3]Southern University of Science and Technology

November 25, 2022

## Abstract

Both shallow and deep groundwater flow mediates a variety of geologic processes. In the discharge zones of the nested groundwater flow systems, saltwater often emerges due to high evaporation (in endorheic drainage basin), tide surge, or marine transgression and regression (in coastal areas) or salt pollution (in streams). However, to our best knowledge there are limited studies that consider the impact of density flow in the discharge zone on the nested groundwater flow systems. In this study, nested groundwater flow systems are analyzed with saltwater infiltration in their discharge zones. To quantify the effects of saltwater concentration on the flow systems, seven scenarios with different saltwater concentrations in the discharge zones are modeled. It is found that the flow systems are most sensitive to the saltwater concentration of the discharge zones when the concentration is between 2.23 and 4 g/L, and the threshold saltwater concentration that starts to affect the flow systems is about 1.35 to 2.23 g/L for the specific aquifer configuration selected for this study. The results also show that the local flow systems retreat upward and the overall groundwater velocity of the entire flow systems is decreased with the increase of the saltwater concentration. This study may shed light on the control of salinization, evolution of saline lake basins, and seawater intrusion from a perspective of nested groundwater flow systems.

# Effects of saltwater infiltration on nested groundwater flow systems

Xiaolang Zhang[1,2], Jiu Jimmy Jiao[1*], Hailong Li[2,3], Xin Luo[1], Xingxing Kuang[2,3]

1. Department of Earth Sciences, The University of Hong Kong, Hong Kong, China
2. School of Environmental Science and Engineering, Southern University of Science and Technology, Shenzhen, 518055, China
3. Guangdong Provincial Key Laboratory of Soil and Groundwater Pollution Control, Southern University of Science and Technology, Shenzhen 518055, China

* Corresponding author Jiu Jimmy Jiao (jjiao@hku.hk). Corresponding address: Department of Earth Sciences, The University of Hong Kong, P. R. China. Room 302, James Lee Science Building, Pokfulam Road, Hong Kong, Tel (852) 2857 8246; Fax (852) 2517 6912

**Abstract**

Both shallow and deep groundwater flow mediates a variety of geologic processes. In the discharge zones of the nested groundwater flow systems, saltwater often emerges due to high evaporation (in endorheic drainage basin), tide surge, or marine transgression and regression (in coastal areas) or salt pollution (in streams). However, to our best knowledge there are limited studies that consider the impact of density flow in the discharge zone on the nested groundwater flow systems. In this study, nested groundwater flow systems are analyzed with saltwater infiltration in their discharge zones. To quantify the effects of saltwater concentration on the flow systems, seven scenarios with different saltwater concentrations in the discharge zones are modeled. It is found that the flow systems are most sensitive to the saltwater concentration of the discharge zones when the concentration is between 2.23 and 4 g/L, and the threshold saltwater concentration that starts to affect the flow systems is about 1.35 to 2.23 g/L for the specific aquifer configuration selected for this study. The results also show that the local flow systems retreat upward and the overall groundwater velocity of the entire flow systems is decreased with the increase of the saltwater concentration. This study may shed light on the control of salinization, evolution of saline lake basins, and seawater intrusion from a perspective of nested groundwater flow systems.

## 1. Introduction

Groundwater flow mediates a variety of geologic, geophysical, and biogeochemical processes in both shallow and deep underground environment [*Schwartz and Domenico*, 1973; *Garven*, 1995; *Person et al.*, 1996; *Stuyfzand*, 1999; *Szijártó et al.*, 2019; *Tóth*, 1999]. Understanding groundwater flow systems is of great practical relevance of ore mineralization [*Garven and Freeze*, 1984; *Garven et al.*, 1993; *Raffensperger and Garven*, 1995; *Garven et al.*, 1999], petroleum migration [*Garven*, 1989], sediment diagenesis [*Lee and Bethke*, 1994], heat transfer [*Szijártó et al.*, 2019], and hydrochemical patterns [*Gupta et al.*, 2015; *Stuyfzand*, 1999] etc.

The foundation of the classical theory of gravity or topography-driven groundwater flow is developed by *Tóth* [1963]. Nested flow systems are initially discussed in the context of an isotropic and homogeneous basin with a water table reflecting the topographic reliefs. Afterwards, the theory is expanded and enriched by many other researchers. Effects of depth-dependent hydraulic conductivity [*Jiang et al.*, 2009; *Cardenas and Jiang*, 2010; *Jiang et al.*, 2010; *Wang et al.*, 2011], anisotropy of hydraulic conductivity [*Freeze and Witherspoon*, 1966; *Wang et al.*, 2011; *Zlotnik et al.*, 2011], water table configuration [*Freeze and Witherspoon*, 1967; *Zhao et al.*, 2018], upper flux boundary [*Liang et al.*, 2013], and layered aquifers [*Gomez-Velez et al.*, 2014] are considered to explore the flow patterns, stagnation zones, groundwater age, local flow penetration depth etc. For a large-scale geological basin, the evolution of regional nested flow systems is also influenced by tectonically-driven compaction, convection flow, fluid production, and dilatancy or seismogenic pumping over a geologic time scale [*Garven*, 1995].

Water in shallow aquifers and surface water bodies may be saline, but the impact of the high-salinity water on the nested flow system has not been studied yet. Saline lakes, marshes, lagoons, and wetlands usually are formed in endorheic basins, arid zones or coastal areas. About ten percent of the earth surface is occupied by such closed or endorheic drainage basins [*Waiser and Robarts*, 2009]. Saltwater bodies occur when water losses from evaporation. For example, in the Badain Jaran Desert in Inner Mongolia, China, there are over 70 lakes among the sand dunes and most of the lakes are saline, with salinity up to 330 g/L [*Jiao et al.*, 2015]. These lakes were speculated to be fresh but become saline gradually in the past few thousand years as a result of climate change. Saltwater bodies are also ubiquitous in shallow aquifers [*Wang and Jiao*, 2012] or lagoons [*Santos et al.*, 2008] in coastal regions due to geological process such as marine transgression and regression [*Han et al.*, 2011] or sea level rise [*Gulley et al.*, 2016] in the recent geological past, or due to catastrophic events like tsunamis or hurricanes [*Jiao and Post.*, 2019], which can turn the freshwater bodies in the low-lying areas into saltwater lakes in a short time.

The denser saltwater may sink and replace the underlying fresh groundwater to reach stability [*Fan et al.*, 1997]. The driving force of a density difference of 1 kg/m$^3$ relative to a reference freshwater density of 1000 kg/m$^3$ is equivalent to a typical groundwater hydraulic gradient of one-meter hydraulic head drop over one-kilometer lateral distance [*Simmons*, 2005]. This calculation shows that a slight saltwater concentration difference is sufficient to reach density driven flow gradients. As a result, the saltwater in the lakes will first modify groundwater flow around the lakes [*Duffy and Al-Hassan* 1988; *Fan et al.*, 1997; *Wooding et al.*, 1997;] and then eventually change the entire flow system when the modification propagates upstream.

Nevertheless, the role of density flow on regional groundwater flow due to saltwater infiltration in the discharge zone of nested groundwater flow systems has not been studied yet. In this study, the theoretical model of regional groundwater flow developed by *Tóth* [1963] is revisited to explore the effects of saltwater infiltration on hydraulic head distribution, flow field, local flow penetration depth, location of the stagnation points, discharge and recharge rate.

## 2. Numerical Analysis on Saltwater Infiltration in a Tóthian Nested Groundwater Flow Systems

Numerical modeling is performed using HydroGeosphere [*Brunner and*

*Simmons*, 2012]. In HydroGeosphere, the saturated subsurface flow is calculated by Darcy's law. The advection-dispersion-diffusion equation is solved for salt transport. Details concerning the theory, governing equations, and numerical solution techniques of HydroGeosphere are introduced by *Therrien et al.*, [2006].

The modeling domain is about 6000 m wide and 1000 m high. Following Tóth [1963], the ground surface of the synthetic basin is defined by the following equation:

$$Z_S(x) = Z_0 + x\tan\alpha + \frac{a}{\cos\alpha}\sin\left(\frac{bx}{\cos\alpha}\right) \quad (1)$$

where $Z_0$=1000 m, $x \in (0, 6000)$, tan$\alpha$=0.02, $a$=15 m and $b$=2π/1500 (Fig. 1). The basin bottom is set at $z$=0. The water table is assumed to mimic the ground surface and thus the water table has the same function as equation (1). The left, right and bottom sides are set as no-flow boundaries. The model domain is laterally discretized at a 15 m resolution, with 50 layers of equal thickness. The grid has 20451 nodes and 20000 elements in the $x$-$z$ plane. In order to determine whether a higher discretization could affect simulation results, simulations with increased discretization (laterally at a 5 m resolution with 80 vertical layers) are carried out. The higher resolution causes negligible differences in saltwater concentration distribution and locations of stagnation points, which indicates that the initial resolution is appropriate to capture the dynamics of salt and water flow.

The solute transport variable is the dimensionless relative saltwater concentration, $c$, changing from 0 to 1 [*Graf and Therrien*, 2005]. It is related with density through the linear equation:

$$\rho_r = \gamma c \quad (2)$$

where $\rho_r$ is the dimensionless relative density, defined by *Frind*, [1982] as:

$$\rho_r = \frac{\rho}{\rho_0} - 1 \quad (3)$$

where $\rho$ [M $L^{-3}$] is the fluid density. The dimensionless constant $\gamma$ is the maximum relative density defined by

$$\gamma = \frac{\rho_{\max}}{\rho_0} - 1 \quad (4)$$

assuming that the saltwater concentration corresponding with the density $\rho = \rho_{\max}$ is $c_{\max} = 1$.

The fluid viscosity also depends on saltwater concentration [*Frey et al.*, 2012]

$$\mu_r = \mu_0 \cdot e^{0.437 C_{DM}} \quad (5)$$

where $\mu_r$ and $\mu_0$ are the dynamic viscosity in saltwater and in fresh water, respectively. $c_{DM}$ is the percentage of solute matter content (%).

At first, a steady state groundwater flow without solute transport is simulated to distinguish the discharge and recharge zones of the domain. Discharge occurs in topographic depressions where salt accumulation often takes places due to evaporation or where saltwater submerges. Then specified concentration boundary is added at the surface of the discharge zone. Saline bodies subjected to evaporation exhibit transient conditions. In this study, saltwater concentration values, 0.5, 1.0, 2.0, 3.0, 4.0, 5.0 and 10.0 g/L are used to investigate the effects of different saltwater concentration in the discharge zone on regional groundwater flow. This setting will help to explore the critical saltwater concentration value at which the boundary concentration in the discharge zone starts to influence the groundwater flow regime. Defining a specific concentration boundary in the discharge zones will help to understand how the increasing rate of boundary saltwater concentration affects the groundwater flow regime. The models run until a steady state for saltwater concentration patterns is achieved.

## 3. Effects of Saltwater Infiltration on the Flow Field

To better understand the effects of saltwater infiltration on groundwater flow patterns, several specific concentrations are defined in the discharge zone of the Tóthian nested groundwater flow systems. Though the groundwater velocity in the discharge zone is upward, salt can still transport downward into the aquifer by free convection, and dissipate via dispersion and diffusion. The modeling results show that as saltwater concentrations increase at the discharge zones of the Tóthian nested groundwater flow systems, the saltwater plumes move further downward (Fig. 2). Though the dominant direction of salt transport is downward, horizontal migration of salt becomes more significant with the increase of penetration depth due to intermediate and regional advection. Once the saltwater moves to reach the intermediate or reginal flow systems (Fig.2c), hrizontal migration of the saltwater plume driven by advection become significant and finilly saltwater from different discharge zones joins with each other and migrates to the lowest discharge zone on the left (Fig. 2d-2g). As a result, down-gradient areas are susceptible to salinization with salt sourced from both local and regional salt trasport. In addition, with different saltwater concentrations at the discharge zone, the routes of saltwater intrusion are almost the same.

The effects of saltwater infiltration on hydraulic head distributions are shown in Fig. 3. The base case for the distributions of hydraulic head is $c$=0 g/L at the discharge zones. Compared with the base case, hydraulic head line densities in the local scale increase with boundary saltwater concentrations. Head line densities in the intermediate and regional scale decrease with boundary saltwater concentrations. In other words, hydraulic gradients are intensified in local scale while those in intermediate and regional scales are reduced. The increasing hydraulic gradients in the local scale are necessary to counterbalance the effect of the density difference to reach a rebalance status. As the hydraulic head contours with a high value shift down-gradient, the head contours in the intermediate and regional scales become sparse. From the perspective of energy conservation, a significant part of energy is used to resist the influence of density difference in the shallow domain, so that the energy to drive intermediate and regional flow systems will be inevitably weakened.

The effects of saltwater infiltration on the flow field are shown in Fig. 4. The velocity is significantly reduced due to salt infiltration. There are two mecahnisms leading to the decrease of groundwater velocity. First, the water density and viscosity are depend on saltwater concentration. Given $c$=10 g/L, the density and viscosity increase to 1.5481 and 1.0074 times of those of fresh water (at temprature 20℃). According to the denifinition of hydraulic conductivity in saturated media, $K=k\rho g/\mu$ (where $k$ is the intrisic conductivity, $g$ is the gravitational acceleration, $\rho$ is the density and $\mu$ is the dynamic viscosity of fluid). The hydraulic conductivity in saltwater decreases to 0.65 times of that in fresh water. The decrease of hydraulic conductivity in saltwater finally leads to the decrease of velocity. Second, pressure head is also depend on the change of saltwater concentration. According to the definition of pressure head $\psi=p/\rho g$ (where $p$ is the fluid pressure), the equivalent fresh water pressure head is $\psi_s=\psi_f\rho_s/\rho_f$ (where $\psi_s$ and $\psi_f$ are pressure head in saltwater and fresh water, respectively; $\rho_s$ and $\rho_f$ are fluid density in saltwater and fresh water, respectively). Thus, given $c$=10 g/L, the pressure head is about 1.0074 times of that in fresh water. The equivalent pressure head is in proportion to the height of saltwater colume. Therefore, as the saltwater infiltrates downward, the saltwater hydraulic head also increases. With a specific saltwater concentration in the discharge zones, the hydraulic gradients decrease accordingly due to the increase of hydraulic head of saltwater in the down-gradient area. According to Darcy's law, both hydraulic conductivity and hydraulic gradient decrease due to salinization, which will ultimately lead to the decrease of velociy.

## 4. Shifts of Stagnation Points and Local Flow Penetration Depth

Once the stagnation points S1-S4 and the streamlines around the four points are pinned, the the local, intermediate, and regional flow systems are also determined [*Wang et al*., 2011]. Thus, the shifts of the stagnation points indicate the transformation of flow systems. Compared with base case in Fig. 4a, the stagnation points and local flows in Figs. 4b-4g are all shifting upward as shown in Fig. 4. The stagnation point S1 and local flows L1 and L2 even move close to the ground surface at $c$=10 g/L (Fig. 4g). Among L3-L9, the shrinking area of L3 is the largest as the saltwater concentration in the discharge zones increases. The change of intermediate flow systems is also noteworthy. Compared with the base in Fig. 4a, the area of IF1 shrinks a little bit and the area of IF2 expandeds in Figs. 4b-4h. There are originally three intermediate flow systems, while IF3 disappears at c=2 g/L and reappears at c=3 g/L. The discharge zone of IF3 is close to L2 at c=1 g/L but close to L1 at c=3 g/L.

To better illustrate how stagnation points change with boundary saltwater concentrations, the variations of dimensionless displacement of four stagnation points in the *x*-direction and *z*-direction with saltwater concentrations are shown in Figs. 5a and 5b, respectively. It is found that the four stagnation points shift upward and leftward. The lateral shift distance normalized to the domain length is very slight. The vertical displacements of the four stagnation points are apparent. S1 can move away from original position and to a distance about 0.3 times of the domain height at $c$=10 g/L.

The dimensionless displacement of stagnation points is non-linear as a function of saltwater concentration. In Fig. 5b, the dimensionless displacement curves of S1, S2, and S3 exhibit three quasi-linear segments. The first segment corresponds to the saltwater concentration at the boundary ranging from 0 to 1 g/L. The slope is gentle, which means that the effects of increment of saltwater concentration in the discharge boundary are limited. The second segment is for saltwater concentration ranging from 1 to 4 g/L. The slope of the second segment is greater than the first one. In this situation, the increment of boundary saltwater concentration has a greater impact on the displacements of stagnation points. The third segment is for saltwater concentration ranging from 5 to 10 g/L. The impacts of the increment of boundary saltwater concentration on the displacements of stagnation points becomes less significant. The dimensionless displacement curve of S4 exhibits two quasi-linear segments. The first segment is where saltwater concentration ranges from 0 to 1 g/L. The slope is gentle as well. The second segment is for saltwater concentration ranging from 1 to 10 g/L. In this case, the impact of the boundary saltwater concentration on the displacements of stagnation points increases with the concentration almost linearly. Based on the development tendency of S1, S2, and S3, as the boundary saltwater concentration increases to a certain value, the slope of the S4 curve will also decrease and the curve should have a third segment.

The variations of dimensionless penetration depth of three local flow systems with saltwater concentrations are shown in Fig. 5c. The curves of penetration depth vs saltwater concentration follow the same pattern as that of displacements of stagnation points S1, S2, and S3 (Fig. 5b). With the increase of saltwater concentration, each curve first increases slowly, then increases rapidly, and finally slowly again. This shows that the shifts of the stagnation points reflect the transformation of flow systems.

Based on Fig. 5, the turning point of the first and second segment occur roughly at $c$=1 g/L. Starting from this concentration, the saltwater infiltration starts to have a significant impact on stagnation point displacement. Regression analysis is carried out to obtain the regression equations for the displacements of the four stagnation points and three local flow penetration depths for seven different concentration conditions at the discharge zones (Table 2). The saltwater concentration value in the discharging zone starts to have an impact on the groundwater flow regime is defined as critical saltwater concentration. Table 1 shows that the intercepts at *c*-axis of these regression equations ranges from 1.35~2.23 g/L. In other words, the critical saltwater concentration ranges from 1.35 to 2.23 g/L. The flow systems are sensitive to the increase of saltwater concentration when concentration ranges from 2.23~4 g/L (Fig. 5). The range of the saltwater concentration in the discharge zones which leads to the greatest changes in displacement of the stagnation points or the changes in the flow systems is important for the management of a specific saline lakes or marshes. This information is useful to control the soil salinization and alkalization, because with this range of saltwater concentration, saltwater infiltrates rapidly, fresh groundwater in deep systems is contaminated by salts, and the aquifer deteriorates quickly.

## 5. Flushing Intensity

*Zlotnik et al.*, [2011] introduced flushing ($F$) to quantitatively measure the flushing intensity over the entire domain. In their expression, the flushing is the averaged velocity over a horizontal line at elevation $z$:

$$F(z)=\frac{1}{L}\int_0^L V(x,z)dx=\frac{1}{L}\int_0^L\left[V_x^2(x,z)+V_z^2(x,z)\right]^{1/2}dx \qquad (6)$$

Since their domain geometry is a rectangle, it's convenient to solve the average velocity mathematically over $z$-plane. In this study, topographic undulation is considered in the numerical model. To simplify the calculation, the flushing is calculated as the averaged velocity over each model layer and $z$ values are the vertical coordinate of the leftmost node of each layer. Flushing can be used to measure velocity damping resulting from the increase in saltwater concentration in the discharge zones.

The results are shown in Fig. 6a. As the boundary saltwater concentration increases, their flushing becomes weak. The decrease of flushing due to the increasing of boundary saltwater concentration is much distinct in shallow system than in deep system, which indicates that the blockage of shallow systems by saltwater infiltration is more intensive. It can be speculated that the residence time of water body is increased correspondingly as a result of blockage of aquifer.

Each flushing intensity curve $F(z)$ displays roughly two quasi-linear segments (Fig. 6a). The substantial change in the slope relates to the depth where the effect of the local systems vanishes. This depth is actually the penetration depth of the local flow systems. Beneath this depth, the flow systems are largely driven by regional head gradients, and undulations of local surface topography become less important. The break points of these curves shift upward as boundary saltwater concentration increases. As shown in Fig. 6a, the distances between two adjacent break points of 1 g/L and 2 g/L, 2 g/L and 3 g/L, 3 g/L and 4 g/L are larger than that between 5 g/L and 10 g/L, indicating that the shrinking of local flow systems is more sensitive to the increase of saltwater concentration when concentration ranging from 1 g/L to 5 g/L. This finding is in consistent with what have been discussed in section 4.

## 6. Recharge and Discharge

At $c$=0 g/L, recharge occurs in local or regional topographic crest and discharge occurs in the topographic depressions, which are separated by hinge lines in Fig. 6b. The hinge line is defined as the boundary between the areas of net recharge and the area of net discharge. The locations of discharge and recharge zones are significantly affected by saltwater infiltration, while it is unaffected by the decrease in hydraulic conductivity with depth [*Jiang et al.*, 2009]. The hinge line shifts to high-elevation places as the boundary concentration increases. In the discharge zones at the base case of $c$=0 g/L, the discharge rate is drastically reduced by saltwater as discussed in section 3. The discharge areas have to be expanded to provide a new water outlet and thus the recharge areas are been reduced. Since discharge rate is reduced and recharge rate has to be decreased (Fig. 6c). Otherwise, recharged water has no-where to escape. It’s noteworthy that two discharge areas occurs at the two sides of the original discharge zones. In these newly expanded discharge area, spring and seepage zone are prone to emerge around the topographic depression. Similar finding was also presented in *Duffy and Al-Hassan’s* [1988] who illustrated that springs emerged along the edge region of the saltwater plays based on their simulated results and field observations,

The decrease of recharge rate in the regional highest places of the domain is not obvious compared to the significant reduction of discharge rate in the regional lowest place is significant. In the high elevation area of the regional slope (the right part of the system as shown in Fig. 2), the contaminated area by saltwater is smaller than that in the low elevation area (the left part of the system in Fig. 2). As saltwater from all the topographic depressions migrates to the left (Fig. 2), overall the saltwater concentration of the groundwater in the system increases progressively to the left. Hence, the variations of discharge and recharge rates increase from the regional upland (left) to the lowland (right).

## 7. Conclusions

The theory of regional flow is developed by *Tóth* [1963] and extended by many researchers. The flow systems affect the properties of solutes, which in turn affect the flow systems. Variable density flow occurs when dense fluid overlies less dense fluid. The variable density effects cause the disturbance of the hydrodynamic conditions of the aquifer system. By adding a specific concentration boundary in the discharge zones of the Tóthian nested groundwater flow systems, density effects on the structure of a topography-driven flow are analyzed. It is found that the local flow systems retreat upward and velocity is increasingly reduced with the increase of the saltwater concentration in the discharge zones. The local flow cell at the lowest elevation is almost replaced by intermediate and regional flow systems at $c$=10 g/L. It is also found that the impact of the saltwater concentration at the discharge zones on the flow systems is not linear. There is a certain threshold of saltwater concentration that starts to affect the flow systems significantly and there is a certain range of the saltwater concentration at the discharge zones that will led to most significant changes of the flow systems. Identifying this saltwater concentration range for a particular flow system is instructive to understand the evolution of the saline lakes and the control of the soil salinization.

**Acknowledgements**

This study was supported by grants from National Natural Science Foundation of China (No. 41572208, 91747204) and the Research Grants Council of Hong Kong (HKU 17304815). The input files and output results of the numerical models are available at Zenodo [*Zhang*, 2020].

## Reference

Brunner, P., and C. T. Simmons (2012), HydroGeoSphere: A Fully Integrated, Physically Based Hydrological Model, *Groundwater*, *50*(2), 170-176, doi:10.1111/j.1745-6584.2011.00882.x.

Cardenas, M. B., and X.-W. Jiang (2010), Groundwater flow, transport, and residence times through topography-driven basins with exponentially decreasing permeability and porosity, *Water Resources Research*, *46*(11), doi:10.1029/2010wr009370.

Cuthbert, M. O., T. Gleeson, N. Moosdorf, K. M. Befus, A. Schneider, J. Hartmann, and B. Lehner (2019), Global patterns and dynamics of climate–groundwater interactions, *Nature Climate Change*, 9(2), 137-141, doi:10.1038/s41558-018-0386-4.

Duffy, C. J., and S. Al-Hassan (1988), Groundwater circulation in a closed desert basin: Topographic scaling and climatic forcing, *Water Resources Research*, 24(10), 1675-1688, doi:10.1029/WR024i010p01675

Fan, Y., C. J. Duffy, and J. Douglas S. Oliver (1997), Density-driven groundwater flow in closed desert basins field investigations and numerical experiments, *Journal of Hydrology*, *196*, 139-184.

Freeze, R. A., and P. A. Witherspoon (1966), Theoretical analysis of regional groundwater flow: 1. analytical and numerical solutions to the mathematical model, *Water Resources Research*, *2*(4), 641-656.

Freeze, R. A., and P. A. Witherspoon (1967), Theoretical analysis of regional groundwater flow. 2. effect of water-table configuration and subsurface permeability variation, *Water Resources Research*, *3*(2), 623-634.

Frey, S. K., D. L. Rudolph, D. R. Lapen, and B. R. Ball Coelho (2012), Viscosity dependent dual-permeability modeling of liquid manure movement in layered, macroporous, tile drained soil, *Water Resources Research*, *48*(6), doi:10.1029/2011wr010809.

Frind, E. O. (1982), Simulation of long-term transient density-dependent transport in groundwater, *Advances in Water Resources*, *5*(2), 73-88.

Garven, G. (1989), A hydrogeologic model for the formation of the giant oil sands deposits of the Western Canada sedimentary basin, *American Journal of Science*, 289, 105-166.

Garven, G. (1995), Continental-scale groundwater flow and geologic process, *Annual Review of Earth and Planetary Sciences*, 23, 89-117.

Garven, G., M. S. Appold, V. I. Toptygina, and T. J. Hazlett (1999), Hydrogeologic modeling of the genesis of carbonate-hosted lead-zinc ores, *Hydrogeology Journal*, 7(1), 108-126, doi:10.1007/s100400050183.

Garven, G., and R. A. Freeze (1984), Theoretical analysis of the role of groundwater flow in the genesis of stratabound ore deposits; 1, Mathematical and numerical model, *American Journal of Science*, 284, 1085-1124.

Garven, G., S. Ge, M. A. Person, and D. A. Sverjensky (1993), Genesis of stratabound ore deposits in the Midcontinent basins of North America; 1, The role of regional groundwater flow, *American Journal of Science*, 293, 497-568.

Gomez-Velez, J. D., S. Krause, and J. L. Wilson (2014), Effect of low-permeability layers on spatial patterns of hyporheic exchange and groundwater upwelling, *Water Resources Research*, *50*(6), 5196-5215, doi:10.1002/2013wr015054.

Graf, T., and R. Therrien (2005), Variable-density groundwater flow and solute transport in porous media containing nonuniform discrete fractures, *Advances in Water Resources*, *28*(12), 1351-1367, doi:10.1016/j.advwatres.2005.04.011.

Gulley, J. D., A. S. Mayer, J. B. Martin, and V. Bedekar (2016), Sea level rise and inundation of island interiors: Assessing impacts of lake formation and evaporation on water resources in arid climates, *Geophysical Research Letters,* 43(18), 9712-9719, doi:10.1002/2016gl070667.

Gupta, I., A. M. Wilson, and B. J. Rostron (2015), Groundwater age, brine migration, and large-scale solute transport in the Alberta Basin, Canada, *Geofluids*, 15(4), 608-620, doi:10.1111/gfl.12131.

Han, D., C. Kohfahl, X. Song, G. Xiao, and J. Yang (2011), Geochemical and isotopic evidence for palaeo-seawater intrusion into the south coast aquifer of Laizhou Bay, China, *Applied Geochemistry*, 26(5), 863-883, doi:10.1016/j.apgeochem.2011.02.007.

Herbert, A. W., C. P. Jackson, and D. A. Lever (1988), Coupled groundwater flow and solute transport with fluid density strongly dependent upon concentration, *Water Resources Research*, *24*(10), 1781-1795.

Herbert, E. R., P. Boon, A. J. Burgin, S. C. Neubauer, R. B. Franklin, M. Ardón, K. N. Hopfensperger, L. P. M. Lamers, and P. Gell (2015), A global perspective on wetland salinization: ecological consequences of a growing threat to freshwater wetlands, *Ecosphere*, 6(10), doi:10.1890/es14-00534.1.

Jiang, X.-W., L. Wan, M. B. Cardenas, S. Ge, and X.-S. Wang (2010), Simultaneous rejuvenation and aging of groundwater in basins due to depth-decaying hydraulic conductivity and porosity, *Geophysical Research Letters*, *37*(5), n/a-n/a, doi:10.1029/2010gl042387.

Jiang, X.-W., L. Wan, X.-S. Wang, S. Ge, and J. Liu (2009), Effect of exponential decay in hydraulic conductivity with depth on regional groundwater flow, *Geophysical Research Letters*, *36*(24), doi:10.1029/2009gl041251.

Jiao, J., and V. Post. (2019), *Coastal Hydrogeology*, New York: Cambridge University Press.

Jiao, J. J., X. Zhang, and X. Wang (2015), Satellite-based estimates of groundwater depletion in the Badain Jaran Desert, China, *Scientific Reports*, 5, 8960, doi:10.1038/srep08960.

Lee, M.-K., and C. M. Bethke (1994), Groundwater flow, late cementation, and petroleum accumulation the Permian Lyons Sandstone, Denver basin, *AAPG Bulletin*, 78(2), 221-241.

Liang, X., D. Quan, M. Jin, Y. Liu, and R. Zhang (2013), Numerical simulation of groundwater flow patterns using flux as upper boundary, *Hydrological Processes*, *27*(24), 3475-3483, doi:10.1002/hyp.9477.

Peck, A. J., and T. Hatton (2003), Salinity and the discharge of salts from catchments in Australia, *Journal of Hydrology*, 272, 191-202.

Person, M., J. P. Raffensperger, S. Ge, and G. Garven (1996), Basin-scale hydrogeologic modeling, *Reviews of Geophysics*, *34*(1), 61-87, doi:10.1029/95rg03286.

Raffensperger, J. P., and G. Garven (1995), The formation of unconformity-type uranium ore deposits; 1, Coupled groundwater flow and heat transport modeling, *American Journal of Science*, 295, 581-636.

Santos, I. R., F. Niencheski, W. Burnett, R. Peterson, J. Chanton, C. F. F. Andrade, I. B. Milani, A. Schmidt, and K. Knoeller (2008), Tracing anthropogenically driven groundwater discharge into a coastal lagoon from southern Brazil, *Journal of Hydrology*, 353(3), 275-293, doi:https://doi.org/10.1016/j.jhydrol.2008.02.010.

Schwartz, F. W., and P. A. Domenico (1973), Simulation of hydrochemical patterns in regional groundwater flow, *Water Resources Research*, *9*(3), 707-720.

Simmons, C. T. (2005), Variable density groundwater flow: From current challenges to future possibilities, *Hydrogeology Journal*, *13*(1), 116-119, doi:10.1007/s10040-004-0408-3.

Stuyfzand, P. J. (1999), Patterns in groundwater chemistry resulting from groundwater flow, *Hydrogeology Journal*, *7*, 15-17.

Szijártó, M., A. Galsa, Á. Tóthb, and J. Mádl-Szőnyi (2019), Numerical investigation of the combined effect of forced and free thermal convection in synthetic groundwater basins, *Journal of Hydrology*, *572*, doi:10.1016/j.jhydrol.2019.03.003.

Therrien, R., R. G. McLaren, E. A. Sudicky, and S. M. Panday (2006), HydroGeoSphere: A Three-Dimensional Numerical Model Describing Fully-Integrated Subsurface and Surface Flow and Solute Transport, *349 pp., Groundwater Simul. Group, Waterloo, Ontario*.

Tóth, J. (1963), A theoretical analysis of groundwater flow in small drainage basins, *Journal of Geophysical Research*, *68*(16), 4795-4812.

Tóth, J. (1999), Groundwater as a geologic agent: An overview of the causes, processes, and manifestations, *Hydrogeology Journal 7*, 1-14.

Waiser, M. J., and R. D. Robarts (2009), Saline Inland Waters, *Encyclopedia of Inland Waters 2*, 634-644.

Wang, X.-S., X.-W. Jiang, L. Wan, S. Ge, and H. Li (2011), A new analytical solution of topography-driven flow in a drainage basin with depth-dependent anisotropy of permeability, *Water Resources Research*, *47*(9), doi:10.1029/2011wr010507.

Wang, Y., and J. J. Jiao (2012), Origin of groundwater salinity and hydrogeochemical processes in the confined Quaternary aquifer of the Pearl River Delta, China, *Journal of Hydrology*, 438-439, 112-124, doi:https://doi.org/10.1016/j.jhydrol.2012.03.008.

Wooding, R. A., S. W. Tyler, and I. White (1997), Convection in groundwater below an evaporating Salt Lake: 1. Onset of instability, *Water Resources Research*, 33(6), 1199-1217, doi:10.1029/96wr03533.

Zhang, Xiaolang. (2020). Effects of saltwater infiltration on nested groundwater flow systems [Data set]. Zenodo. http://doi.org/10.5281/zenodo.3601733

Zhao, K.-Y., X.-W. Jiang, X.-S. Wang, L. Wan, J.-Z. Wang, H. Wang, and H. Li (2018), An analytical study on nested flow systems in a Tóthian basin with a periodically changing water table, *Journal of Hydrology*, *556*, 813-823, doi:10.1016/j.jhydrol.2016.09.051.

Zlotnik, V. A., M. B. Cardenas, and D. Toundykov (2011), Effects of multiscale anisotropy on basin and hyporheic groundwater flow, *Groundwater*, *49*(4), 576-583, doi:10.1111/j.1745-6584.2010.00775.x.

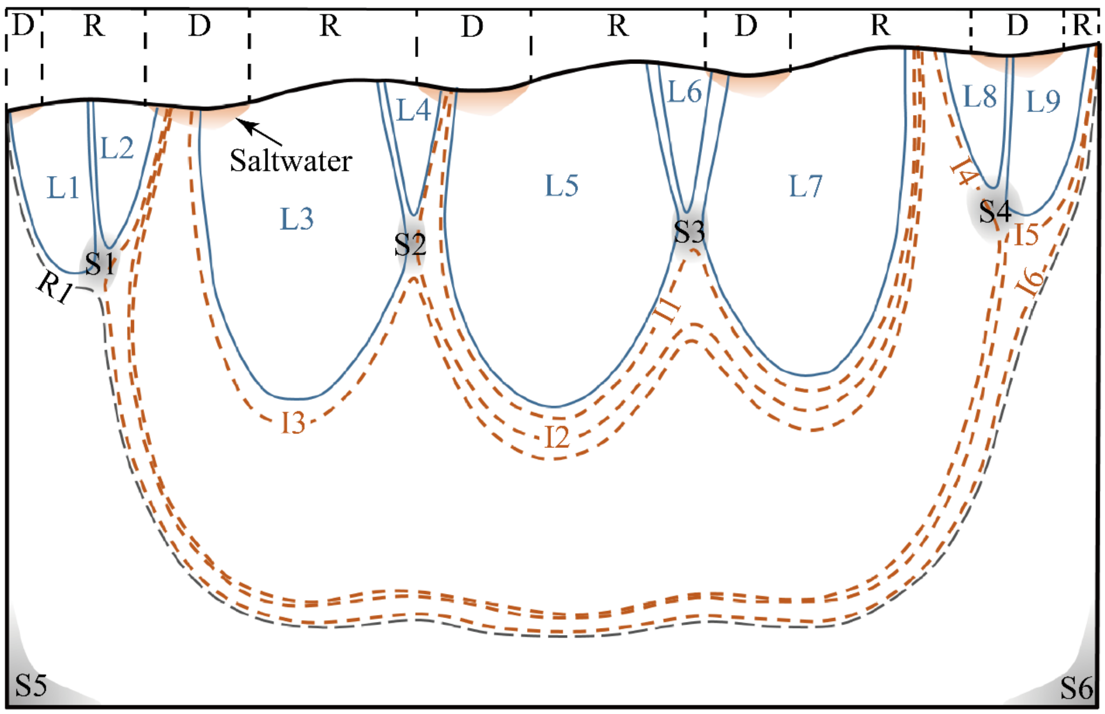


Fig. 1. Theoretical model with saltwater infiltration. S1 to S6 denote the stagnation points. In this study, total 16 streamlines close to stagnation points S1-S4, including 9 local streamlines, 6 intermediate streamlines, and 1 regional streamline, are enough to divide the flow systems. Owing to the periodic undulations of the water table, there are nine local flow systems (from L1 through L9). Intermediate flow system IF1, IF2, and IF3 are divided by streamlines I1 and I2, I3 and I4, I5 and I6, respectively. The domain below streamline R1 is occupied by regional flow. The orange areas near the water table show the high salinity zone due to saltwater infiltration. D and R denote discharge and recharge zones, respectively.

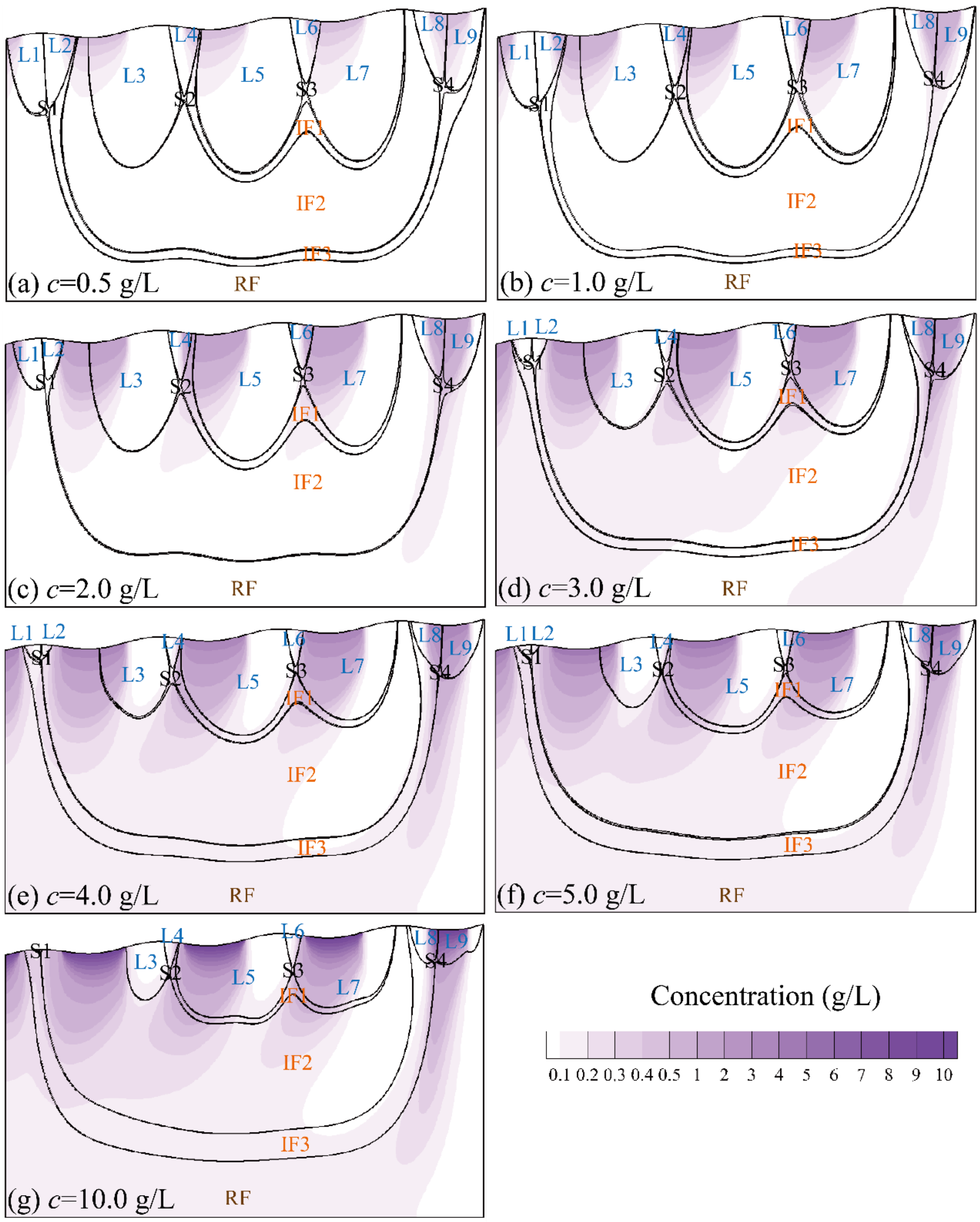


Fig. 2 Distributions of saltwater concentrations resulting from different boundary saltwater concentrations $c$ in the discharge zones. L, IF, and RF denote the local, intermediate, and regional groundwater flow system, respectively.

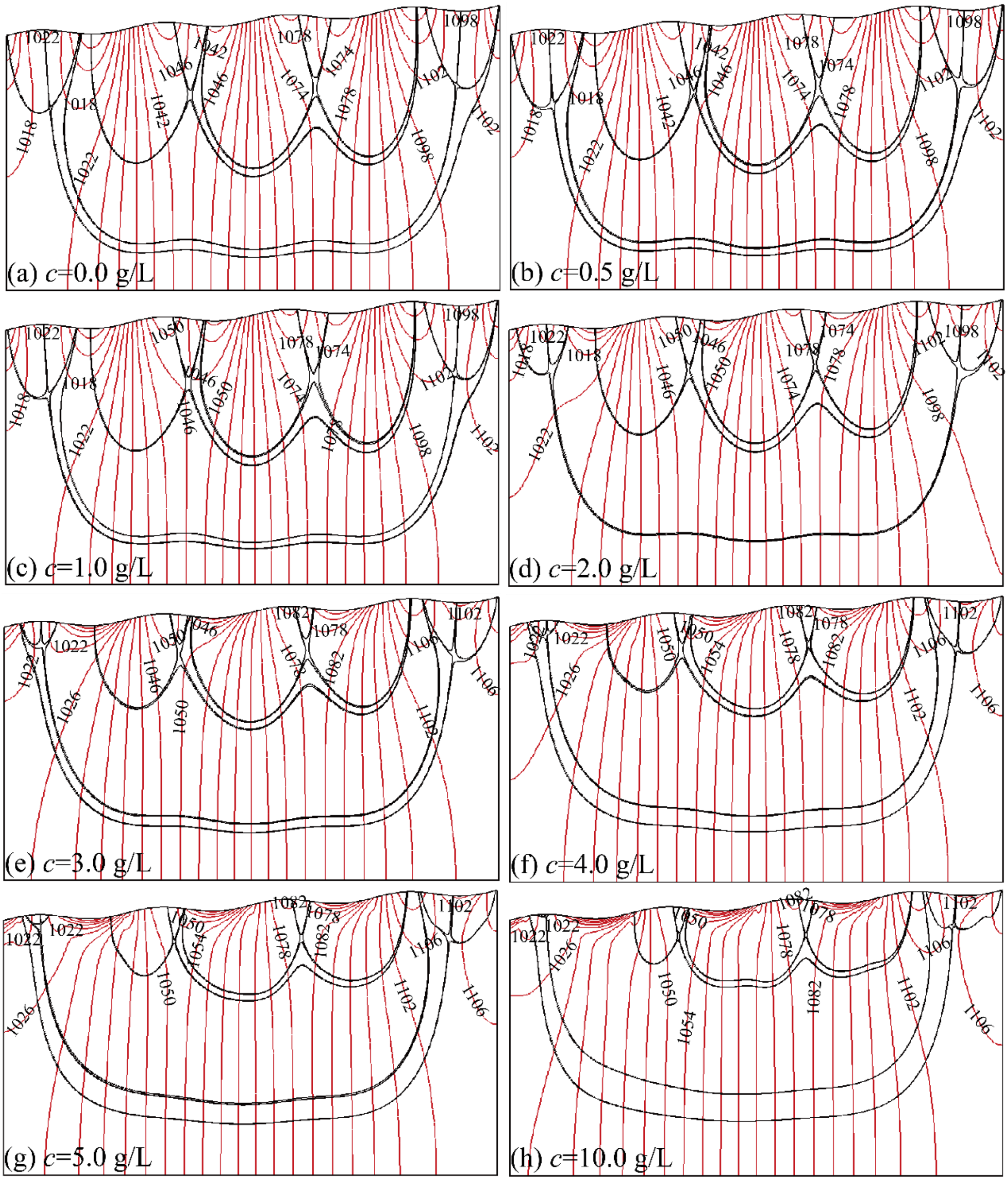


Fig. 3 Distributions of hydraulic head (red) (m) at 4 m increment and streamlines (black) resulting from different boundary saltwater concentrations *c* in the discharge zones.

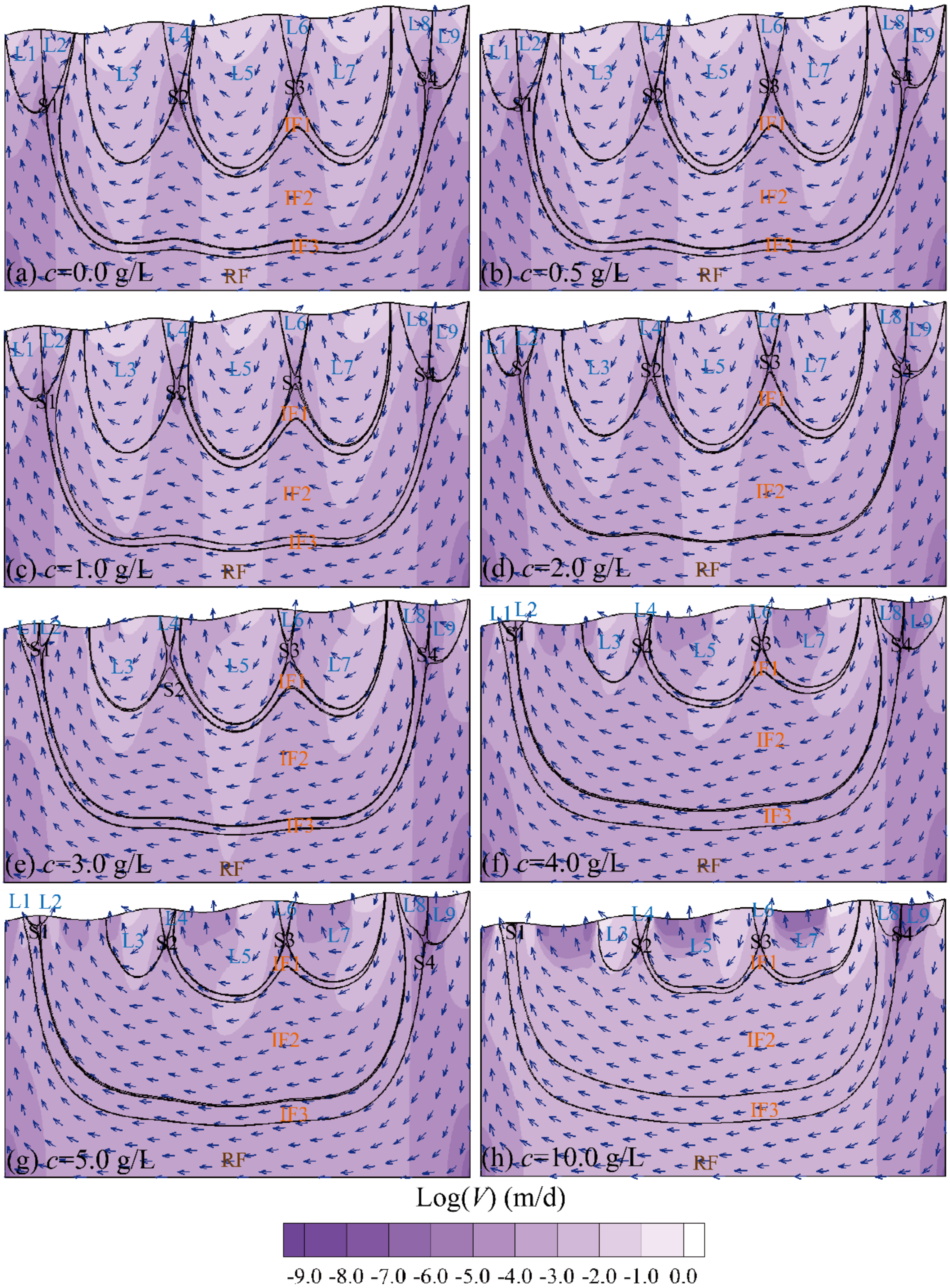


Fig. 4 Darcy velocity magnitude $V$ (m/s) contours, streamlines (black) and velocity field (blue) resulting from different boundary saltwater concentrations $c$ in the discharge zones. L, IF, and RF denote the local, intermediate, and regional groundwater flow system, respectively.

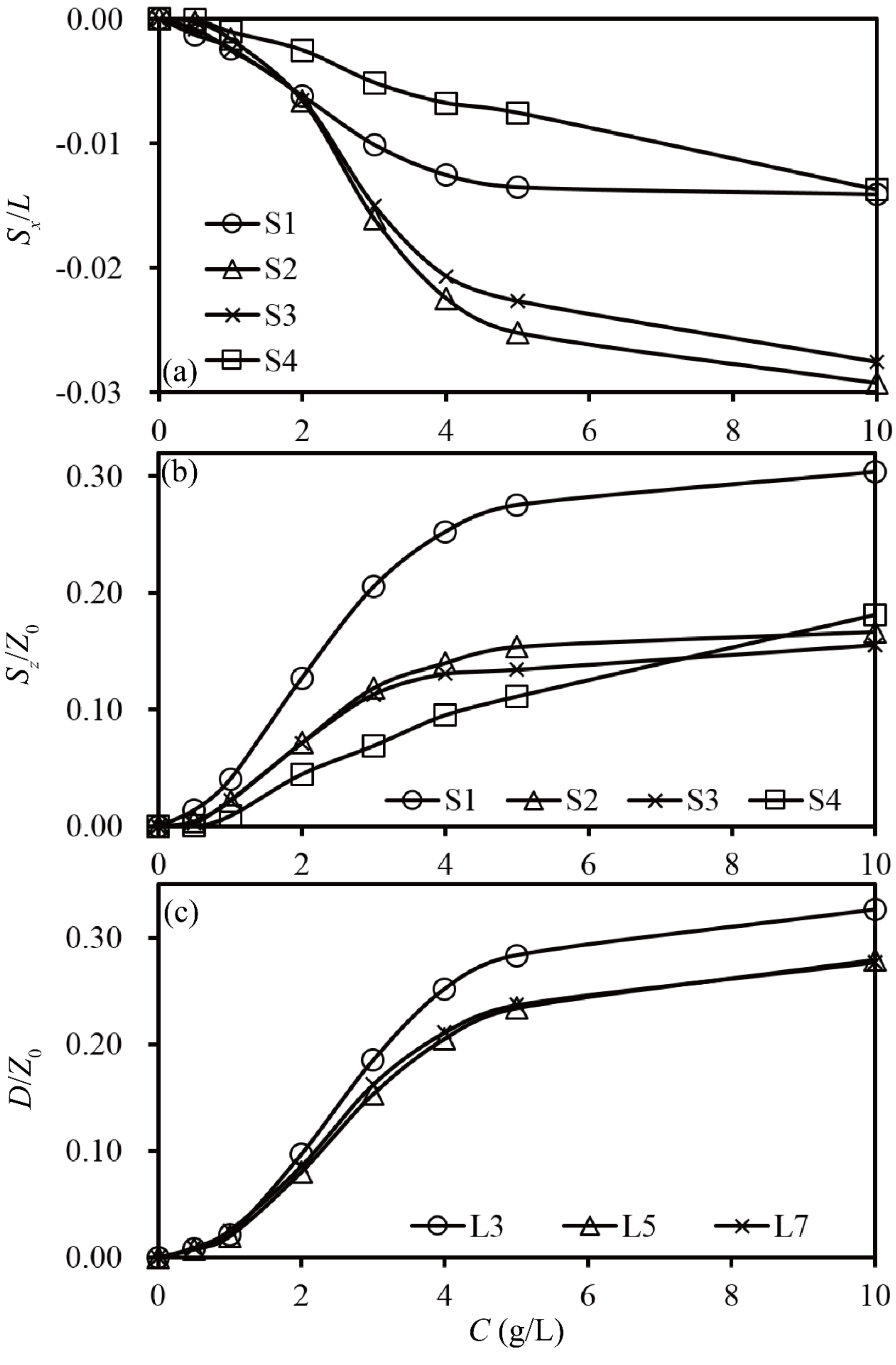


Fig. 5. Displacements of stagnation points and local flow penetration depth.

The variations of dimensionless displacements of four stagnation points in the $x$-direction (a) and in the $z$-direction (b) with saltwater concentrations , respectively ($L$=6000 m and $Z_0$=1000 m). (c) The variations of dimensionless displacements of penetration depth of three local flow systems with saltwater concentrations. The locations of S1, S2, S3, and S4 and L3, L5, and L7 are shown in Fig. 1.

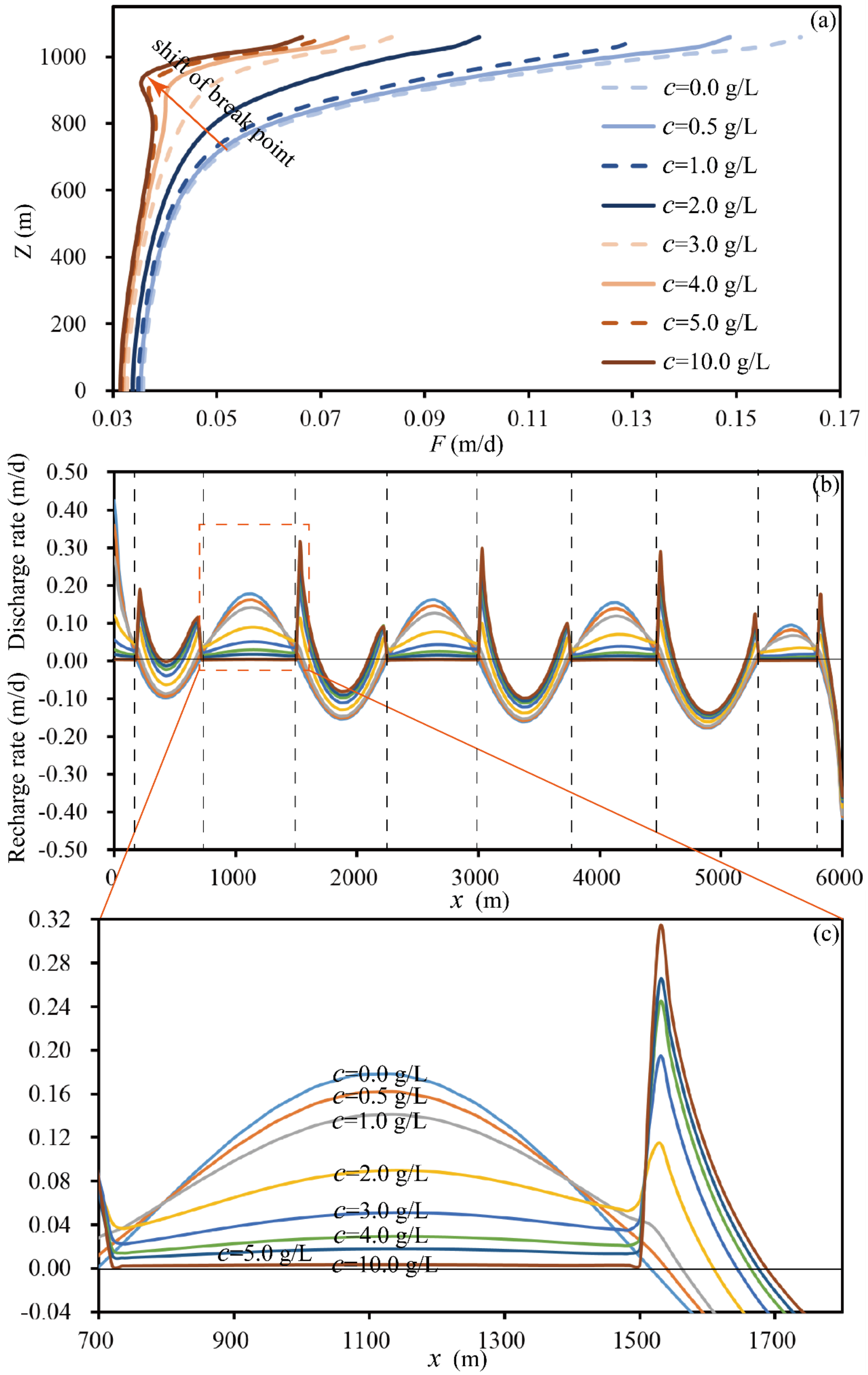


38

39 Fig. 6. (a) Flushing intensity ($F$) profiles for different saltwater

concentrations in the discharge zones. (b) and (c) recharge and discharge rate distribution (m/d) at the upper boundary of the domain.

Table 1. HydroGeosphere Model Parameter Values and Attributes

| Description | Value | Unit | Reference |
|---|---|---|---|
| Hydraulic conductivity | 1 | m/d | Jiang et al., [2009] |
| Longitudinal dispersivity | 10 | m | giving the local scaled dispersivity 10÷(6000÷9)=0.015, referred from Fan et al. [1997] |
| Lateral dispersivity | 1 | m | giving lateral dispersivity/longitudinal dispersivity=0.1 |
| Molecular diffusion coefficient | $8.64\times10^{-6}$ | $m^2/d$ | |
| porosity | 0.375 | — | typical value for silt |
| Fresh water density | 998.402 | $kg/m^3$ | |
| Fresh water viscosity | 86.54 | Pa·d | fresh water dynamic viscosity at 20℃ |
| Maximum saltwater concentration | 10 | g/L | |
| Maximum saltwater viscosity | 133.966 | Pa·d | from Eq. (5) |
| Maximum saltwater density | 1005.81 | $kg/m^3$ | from *El-Dessouky and Ettouney*, [2002] |

Table 2. $S_x/L$ (dimensionless displacements of stagnation points in the $x$-direction), $S_z/Z_0$, (dimensionless displacements of stagnation points in the $z$-direction), and $D/Z_0$ (dimensionless displacements of penetration depth of local flow systems) for different concentration, regression equations, and intercepts of the equations at $c$-axis (The locations of S1, S2, S3, and S4 and L3, L5, and L7 are shown in Fig. 1; $L$=6000 m and $Z_0$=1000 m)

| | | Saltwater concentration (g/L) in the discharge zones | | | | | | | Regression equation | Intercept at $c$-axis |
|---|---|---|---|---|---|---|---|---|---|---|
| | | 0.5 | 1 | 2 | 3 | 4 | 5 | 10 | | |
| $S_x/L$ | S1 | -0.0013 | -0.0024 | -0.0062 | -0.0101 | -0.0125 | -0.0135 | -0.0141 | $y = -0.004\ln(c) - 0.0012$ $R^2 = 0.89$ | 1.35 |
| | S2 | -0.0002 | -0.0016 | -0.0066 | -0.0161 | -0.0224 | -0.0252 | -0.0292 | $y = -0.005\ln(c) - 0.004$ $R^2 = 0.93$ | 2.23 |
| | S3 | -0.0008 | -0.0025 | -0.0065 | -0.0150 | -0.0207 | -0.0226 | -0.0275 | $y = -0.01\ln(c) - 0.0045$ $R^2 = 0.93$ | 1.51 |
| | S4 | 0.0000 | -0.0010 | -0.0025 | -0.0051 | -0.0067 | -0.0075 | -0.0137 | $y = -0.011\ln(c) - 0.0043$ $R^2 = 0.92$ | 1.48 |
| | | 0.5 | 1 | 2 | 3 | 4 | 5 | 10 | | |
| $S_z/Z_0$ | S1 | 0.0140 | 0.0402 | 0.1269 | 0.2052 | 0.2523 | 0.2753 | 0.3038 | $y = 0.1113\ln(c) + 0.0722$ $R^2 = 0.95$ | 1.91 |
| | S2 | 0.0043 | 0.0217 | 0.0714 | 0.1184 | 0.1398 | 0.1539 | 0.1667 | $y = 0.0626\ln(c) + 0.0394$ $R^2 = 0.95$ | 1.88 |
| | S3 | 0.0028 | 0.0221 | 0.0711 | 0.1129 | 0.1307 | 0.1342 | 0.1555 | $y = 0.0573\ln(c) + 0.0375$ $R^2 = 0.96$ | 1.92 |
| | S4 | 0.0002 | 0.0089 | 0.0446 | 0.0688 | 0.0952 | 0.1111 | 0.1670 | $y = 0.0568\ln(c) + 0.0189$ $R^2 = 0.94$ | 1.39 |
| | | 0.5 | 1 | 2 | 3 | 4 | 5 | 10 | | |
| $D/Z_0$ | L3 | 0.0081 | 0.0216 | 0.0970 | 0.1851 | 0.2520 | 0.2832 | 0.3260 | $y = 0.122\ln(c) + 0.0561$ $R^2 = 0.94$ | 1.58 |
| | L5 | 0.0077 | 0.0199 | 0.0803 | 0.1533 | 0.2052 | 0.2338 | 0.2791 | $y = 0.1022\ln(c) + 0.0465$ $R^2 = 0.94$ | 1.58 |
| | L7 | 0.0092 | 0.0255 | 0.0859 | 0.1623 | 0.2112 | 0.2368 | 0.2771 | $y = 0.1014\ln(c) + 0.0513$ $R^2 = 0.95$ | 1.66 |

49